Artificial Thickening of a Transonic Boundary Layer in the Presence of a Pressure Gradient Associated with a Boundary Layer Ingestion Concept

Gregory S. Jones[1], William Milholen[2], Alaa Elmiligui[2], Michael Bozeman[3], Christopher Cramer[4], Mark Cagle[5]

NASA Langley Research Center, Hampton, Virginia, 23681

Boundary layer ingestion is an aeropropulsive concept associated with a propulsion airframe integration technique that integrates viscous aerodynamics into a propulsion system to achieve more efficient flight. The effectiveness of this concept is heavily dependent on how much of the boundary layer is being ingested into the propulsor. Scaling this concept for transonic wind tunnel testing is often plagued with blockage issues and requires a modification to the model dimensions such as fuselage length and diameter and wingspan. To simulate the boundary layer for these modified models requires a manipulation of the boundary layer height to achieve the appropriate ratio of boundary layer to propulsor inlet diameter or height. This paper will focus on 15 different transonic boundary layer manipulators to achieve varying turbulent boundary layer heights for a representative single-aisle transport utilizing Boundary Layer Ingestion.

Nomenclature

BLI = Boundary Layer Ingestion
CFD = Computational Fluid Dynamics
C_p = pressure coefficient
F = frequency (Hz)
Δf = frequency resolution (Hz)
H = shape factor
L = length (feet or inches)
M = wind tunnel Mach number
P_O = free stream total pressure (psi)
P_∞ = free stream static pressure (psi)
P_S = model surface static pressure (psi)
p' = unsteady pressure (psig)
Re = unit Reynolds number (per foot)
Re_L = Reynolds number (based on reference length, L)
q = dynamic pressure (psi)
TCT = Transonic Cryogenic Tunnel
T_O = free stream total temperature (°F)
U = velocity (ft/sec)
V = specific volume = $1/\rho$
δ^* = boundary layer displacement thickness
θ = boundary layer momentum thickness
ρ = local fluid density
κ = Von Karman constant
ε = thermodynamic property of real gas

[1] Senior Research Engineer, Configuration Aerodynamics Branch, AIAA Associate Fellow.
[2] Senior Research Engineer, Configuration Aerodynamics Branch, AIAA Senior Member.
[3] Research Engineer, Configuration Aerodynamics Branch, AIAA Member.
[4] Test Engineer, Sierra Lobo, Inc., Subsonic/Transonic Test Branch.
[5] Design Engineer, Aeronautics System Engineering Branch.

Introduction

Boundary layer ingestion (BLI) is an aeropropulsive concept that integrates the aerodynamics and propulsion system of an aircraft to achieve more efficient flight. The basic concept is that the propulsion system can produce the same thrust for less input power by ingesting air that has been decelerated via viscous effects in the boundary layer around the aircraft. NASA has recently developed the Single-Aisle Turboelectric Aircraft Concept (STARC-ABL)[1,2] that is based on the

Figure 1. Tailcone propulsor concept with full annular BLI.

BLI of a full annular or radial ingestion distributed into a propulsor as shown in Figure 1. The benefit of BLI is based on the amount of the boundary layer being ingested by the propulsor. The largest impact is seen at the root of the fan where the maximum boundary layer momentum occurs. Sizing the propulsor will be based on the height of the boundary layer being ingested, which will be a function of the fuselage length and influence of the wing downwash. The purpose of this effort is to provide an experimental database for generating the boundary layer characteristics and pressure gradients of a single-aisle transport on a representative cylindrical body with a reduced fuselage length. While this effort does not include the effects of a powered propulsor or wing downwash, it does provide a mechanism for effectively changing the boundary layer and propulsor sizing for future powered testing.

This paper will focus on the development of the boundary layer on a semispan representation of an afterbody without a vertical tail in the NASA 0.3m Transonic Cryogenic Tunnel (TCT).[3] The current model is a 1.82% scale of the full-scale afterbody so that it would fit into the 0.3m TCT. Test conditions for this experiment included Mach numbers ranging from 0.2 to 0.9 and unit Reynolds number from 1.34×10^6/ft to 28.7×10^6/ft. A CFD comparison of the 0.3m TCT boundary layer growth of the full-length configuration and the shortened fuselage configuration without boundary layer manipulators is shown in Figure 2. A goal of this effort is to manipulate a boundary layer that will enable BLI on a modified/shortened fuselage that is representative of a full-length fuselage. A companion paper will describe the CFD effort[4] associated with this experimental work.

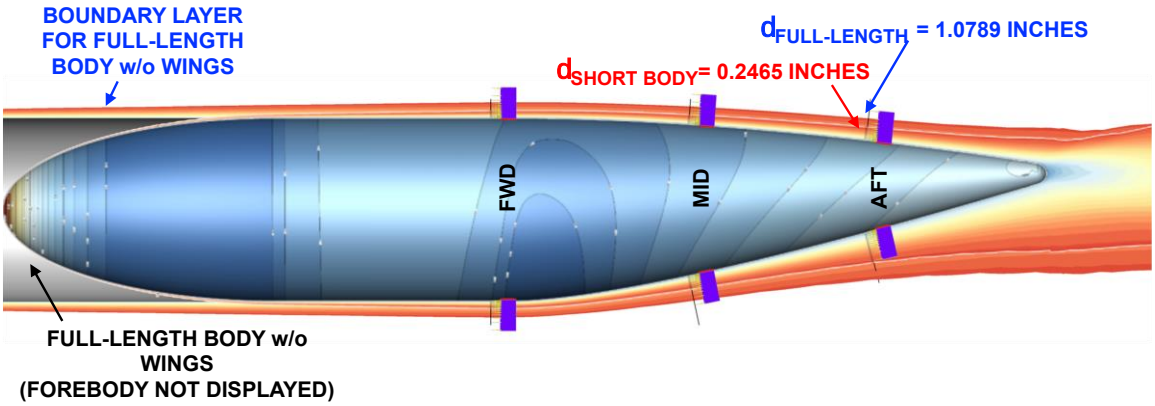

Figure 2. CFD comparison of 0.3m TCT scaled boundary layer growth for full length

Boundary Layer Characteristics

The fundamental requirement for this study was to create a turbulent boundary layer that has the characteristics of a naturally developed turbulent boundary layer[5] on the afterbody of the model. The shape factor, *H*, is defined as the ratio of displacement thickness to momentum thickness,

$$H = \frac{\delta^*}{\theta} \tag{1}$$

where the displacement thickness is:

$$\theta = \int_0^{\delta} \frac{\rho U}{\rho_\infty U_\infty}\left(1 - \frac{U}{U_\infty}\right) dz \tag{3}$$

and the momentum thickness is:

$$\theta = \int_0^{\delta} \frac{\rho U}{\rho_\infty U_\infty}\left(1 - \frac{U}{U_\infty}\right) dz \tag{3}$$

and ρ is the local density, ρ_∞ is the freestream density, U is the local velocity in the streamwise direction, U_∞ is the freestream velocity, and δ is the distance in the z-direction corresponding to $U = 0.99\ U_\infty$. The shape factor for a fully developed flat plate boundary layer, $H = 2.59$ (Blasius boundary layer) is typical of laminar flows, while $H = 1.3$ - 1.4 is typical of turbulent flows.[6] It should be noted that an adverse pressure gradient can reduce the Reynolds number at which transition into a fully turbulent boundary layer may occur.

Two approaches were used to curve fit the measured boundary layer profiles; (1) the Law of the Wall[7] and (2) a Velocity Power Law[8,9]. The most widely used law of the wall function is the logarithmic law which has the form:

$$u^+ = \frac{1}{\kappa} ln(y^+) + B \tag{4}$$

where κ is the Von Karman constant and B is the constant of integration. Spaulding developed a special form of this equation to satisfy the no-slip equation:

$$y^+ = u^+ + A\left[e^{\kappa u^+} - 1 - \kappa u^+ - \frac{(\kappa u^+)^2}{2} - \frac{(\kappa u^+)^3}{6} - \frac{(\kappa u^+)^4}{24}\right] \tag{5}$$

where $A = e^{-\kappa u^+} = 0.1108,\ \kappa = 0.4,$ and $B = 5.5.$

Semispan Model

A semispan model was built in two interchangeable configurations consisting of top and bottom views of the fuselage. Each configuration had removable rakes to measure total pressure and could be located at three streamwise locations and three radial locations as shown in Figure 3. These locations were chosen to document the downstream development of the modified boundary layer, and determine the distance required to obtain a fully mixed boundary layer. Three rakes were used at one streamwise location at a time. Each rake contained 15 total pressure probes as seen in Figure 4. The semispan model has a maximum length of 26.8 and a maximum diameter of 4.7 inches. The forebody of the semispan model has a 3:1 elliptical profile. There is a 0.5-inch standoff at the base of the model to minimize the effects of the tunnel wall boundary layer. To evaluate the impact of the various manipulators on the boundary layer measured by the rakes, an interchangeable manipulator is located at x/L=0.26.8 (7.175 inches from the leading edge).

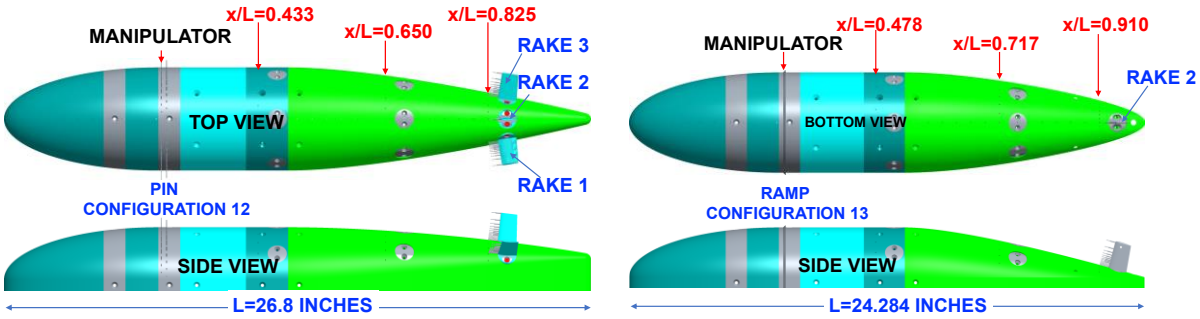

Figure 3. Semispan model highlighting the various rake locations.

Figure 4. Total pressure probe distribution of installed rake.

Boundary Layer Manipulators

This experiment was performed to evaluate the boundary layers resulting from a variety of manipulators at transonic Mach numbers and Reynolds numbers characteristic of flight. The goal was to identify manipulators that provide thickened boundary layers that meet the following criteria: (1) the profile of the thickened boundary layer shall have the characteristics of a fully developed turbulent boundary layer, (2) grow a turbulent boundary layer to a scaled height that is consistent with a full scale single-aisle aircraft, (3) the frequency spectrum of the fluctuating static pressure shall have a random distribution without discrete energy spikes, and (4) the measured fluctuating variables associated with the thickened boundary layer shall agree with those characteristics of natural boundary layers.

A baseline configuration and 14 different manipulators including both pin configurations and 45° ramps were evaluated. Figure 5 illustrates an example of the baseline, a variable height pinned configuration, and a ramp configuration. The initial manipulator design (configuration 8) was based on a 1976 Otten[10,11] study of pin thickeners on a flat plate. The manipulator selections for this study were expanded to include ramps that achieve similar boundary layer performance with smaller protrusions into the flow.

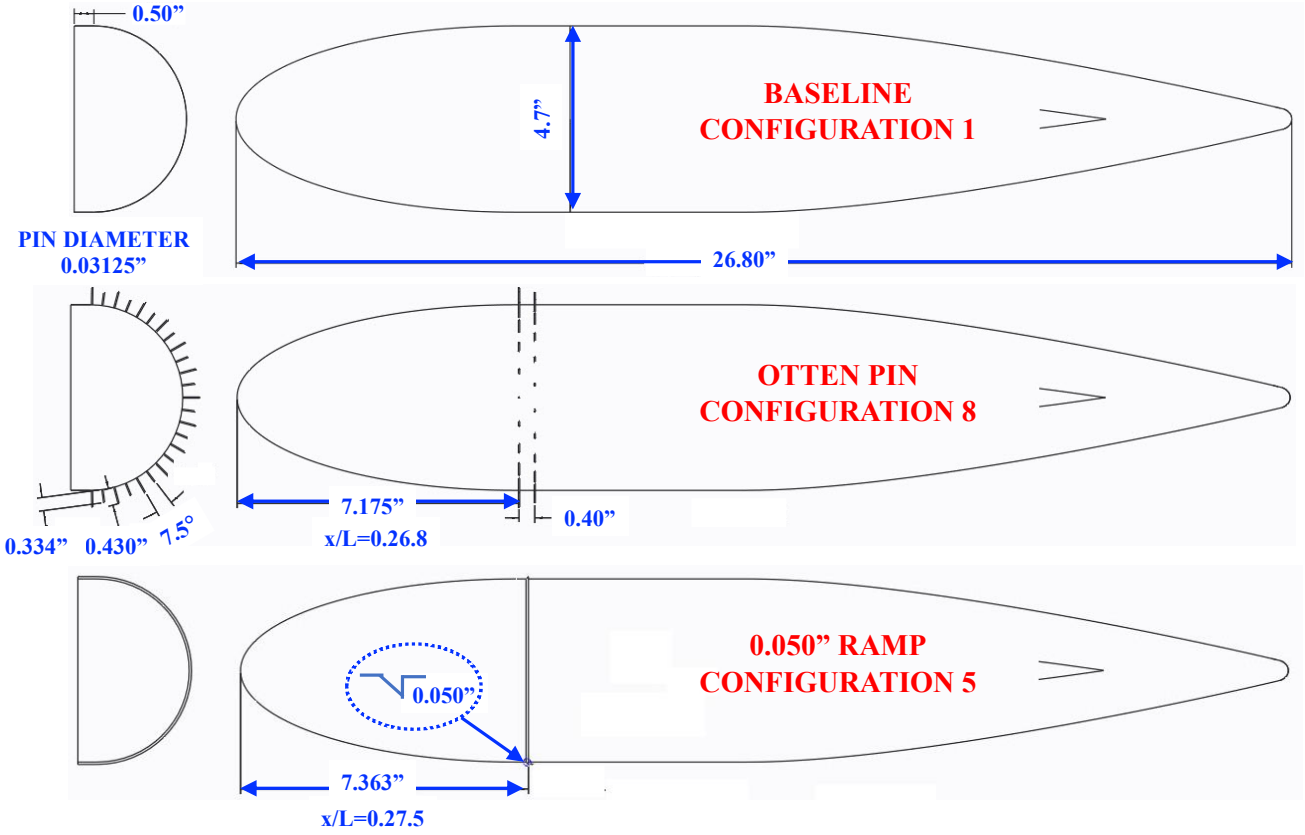

Figure 5. Example of boundary layer manipulator configurations (Top View).

Facility

The 0.3m TCT is a high pressure, closed circuit, cryogenic, transonic wind tunnel (Figure 6) that can independently vary Mach number and Reynolds number[12,13]. The operational characteristics of the tunnel are shown in Table 1. The manipulator test envelope shown in Figure 7 highlights the Mach number and required Reynolds number conditions for the current test. The 0.3m TCT test section has a cross section of 13 inches by 13 inches and is 70.38 inches long. It also features upper and lower flexible walls that can be used to optimize the farfield streamlines to minimize wall interference and blockage effects. The wall settings for this model are highlighted in Figure 8.

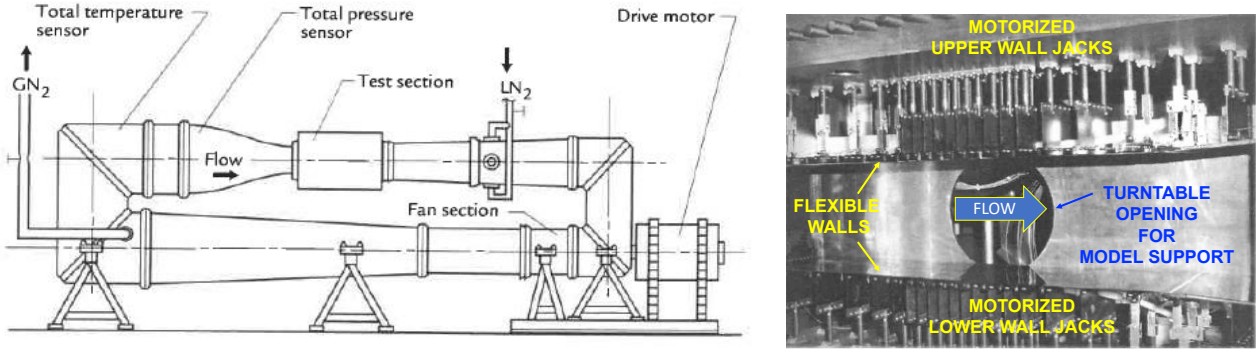

a) Schematic of the 0.3m TCT. b) Photo of Test Section

Figure 6. Diagram and photo of the 0.3m TCT.

Table 1. 0.3m TCT Operational Characteristics.

Mach	0.1 to 0.9	± 0.001
Re/ft	up to 100×10^6	
PTo, psia	14.7 to 88	± 0.0440 ± 0.0073
To, °F	(-320) to 130	± 2

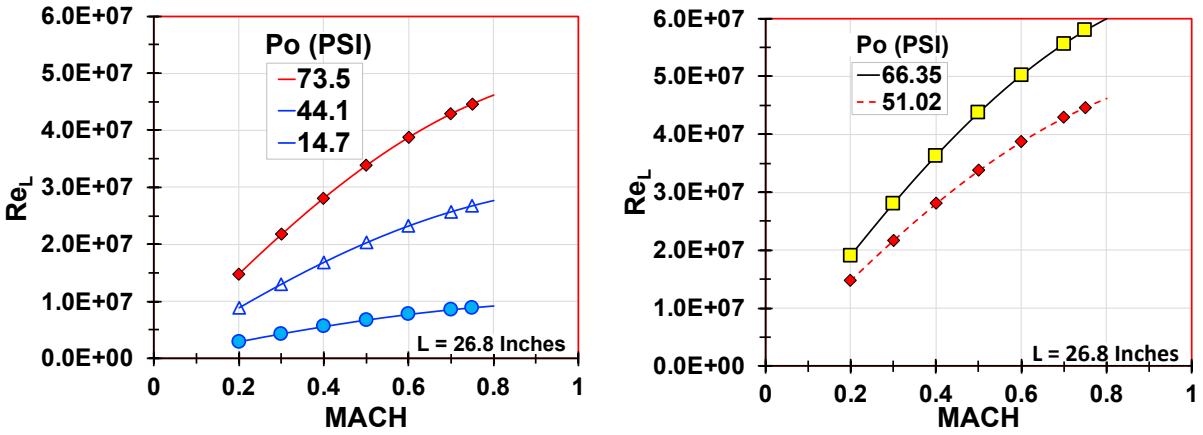

a) Warm Nitrogen Mode (To=80°F) b) Cold (To=-50°F)

Figure 7. TCT test envelope for two total temperatures.

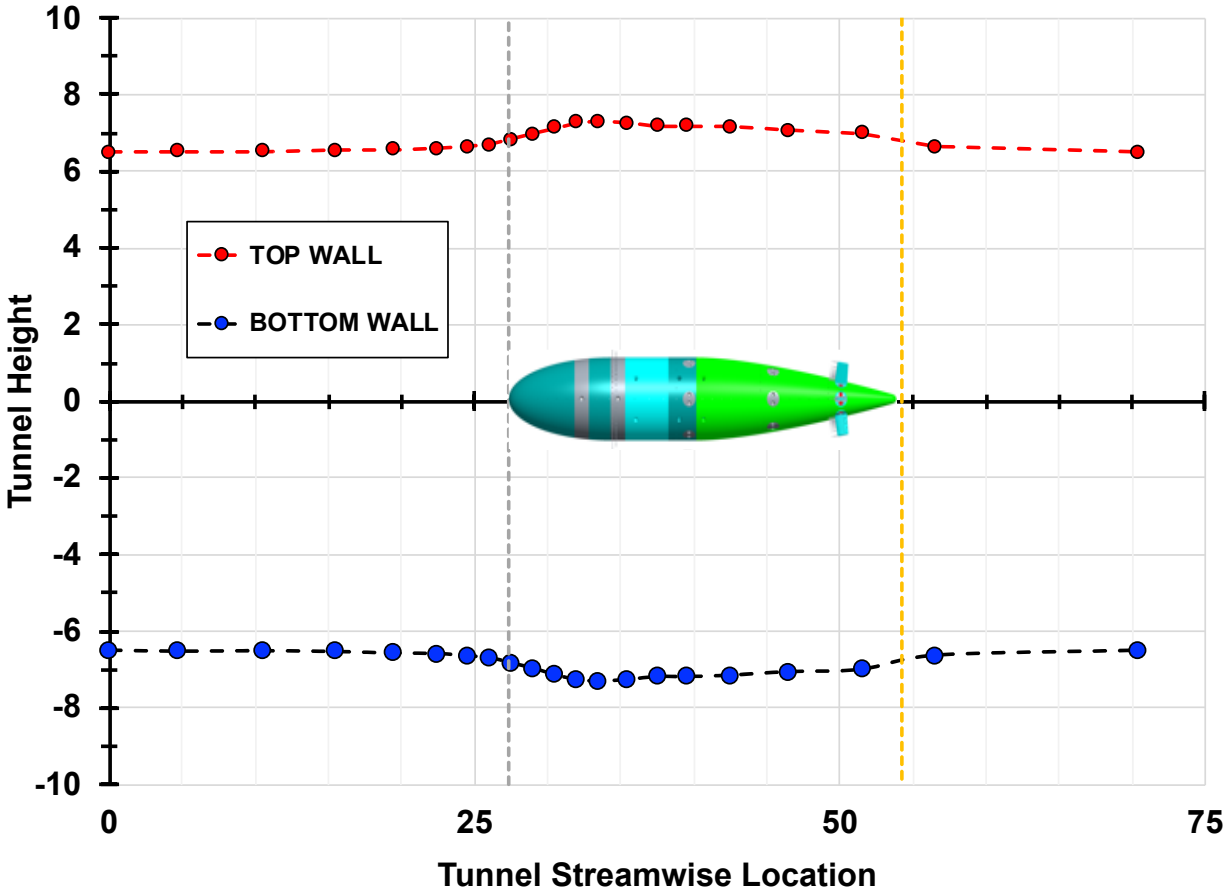

Figure 8. Test section wall geometry optimized for the this semispan model.

To achieve the flight Reynolds number for this test, density was varied by managing total temperature and total pressure for a given Mach number. These tunnel parameters use the real gas equations rather than the ideal gas equations used at most facilities. In the 0.3m TCT data reduction software[14], the gaseous properties for both air and nitrogen are mathematically represented by the Beattie-Bridgeman[15] thermal equation of state which has the form:

$$P = \left(\frac{RT(1-\varepsilon)}{V^2}\right)(V+B) - \left(\frac{A}{V^2}\right) \quad (6)$$

The data reduction calculations require three inputs that include measured tunnel total pressure, total temperature, and static pressure at the beginning of the test section. All test conditions utilized the nitrogen mode so the real gas equations for this test are all based on the operating environment of nitrogen.

Results

The model measurements taken for this test included centerline static pressure, radial static pressure, pitot pressure at the rake locations, and static pressure distributions on the tunnel walls. The centerline static pressure measurements for four different manipulators for Mach numbers of 0.7, 0.75, and 0.8 are illustrated in Figure 9. The results show that little difference is observed for the three Mach numbers shown. Each manipulator has a localized effect on the model surface pressure, and the effect grows with the height of the manipulator. The pressure distribution downstream of x/L=0.5 is nearly identical for all of the cases. Additionally, the rake measurements

show a spike in the static surface pressure resulting from the presence of the rakes. The development of the boundary layer is also influenced by the juncture flow near the stand-off of the model.

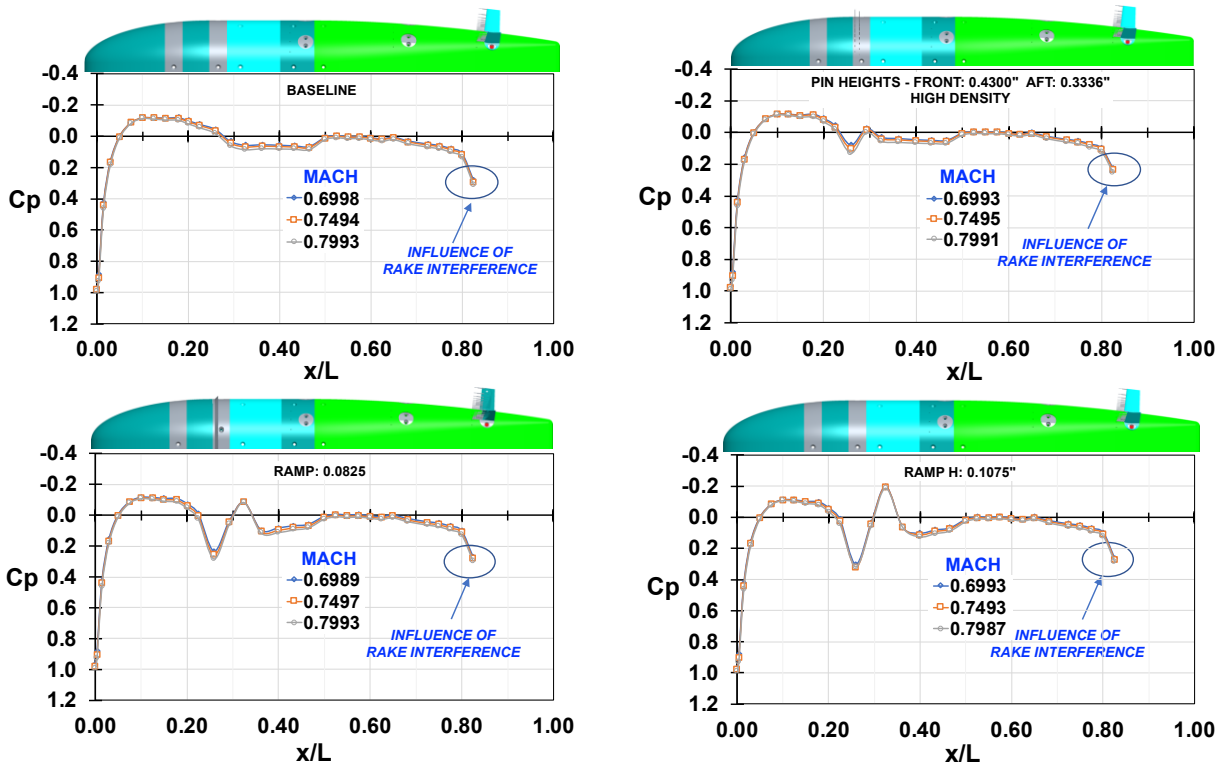

Figure 9. Pressure distribution for four boundary layer manipulator for the top view

This variation is represented by radial surface pressure as shown in Figure 10. To minimize the influence of the rake on the surface pressure used to calculate the local rake velocity, an averaged surface pressure was calculated utilizing a limited radial distribution (equation 7).

$$Ps_{AVG} = \frac{P_{-45°}+P_{-30°}+P_{-15°}+P_{15°}+P_{30°}+P_{45°}}{6} \quad (7)$$

The asymmetry in the radial static profiles can also be seen in the boundary layer rake total pressure profiles shown in Figure 11 and can be attributed to asymmetries in the wall setting described above. Comparing the baseline and ramp configurations, the impact of the wall influences the growth of the boundary layer more on the ramp configuration than the baseline resulting in a smaller boundary layer along the centerline (Rake 2) than the off-axis profiles.

The solid blockage of the model is 6.52% and influences the free stream velocity distribution in the test section and the edge velocity of the boundary layer profiles. This is illustrated in Figure 12 by the variation in static pressure distributions on the top wall as a function of Mach number. While the solid walls were adjusted for this configuration, it should be noted that nominal wall settings are for 2-D airfoil applications, not 3-D bluff bodies. Therefore, to make accurate comparisons to this experimental data set, it will be necessary to include the influence of the walls.

The influence of the manipulated boundary layer growth is a function of the manipulator height, radial distribution, and model pressure gradient. Using an approach suggested by Klebanoff and Diehl,[16] mean velocity profiles were used as a basis for comparison of the different manipulators. The measured boundary layers were obtained at three streamwise locations, x/L=0.433, x/L=0.650, x/L=0.825; and referenced to the leading edge of the model. To ensure that the boundary layer was turbulent; the

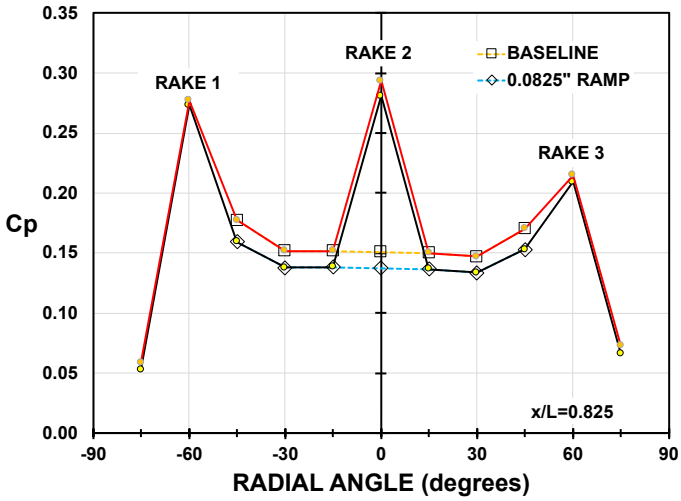

Figure 10. Examples of surface pressure profiles for different radial rake locations, Mach=0.75, Re =26x10^6/ft.

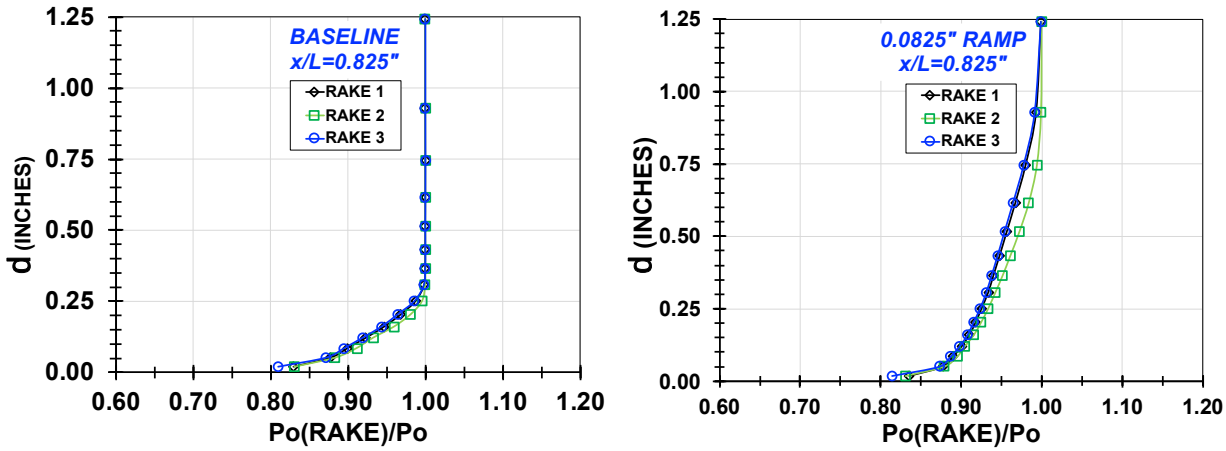

Figure 11. Pressure profiles for different radial rake locations, baseline configuration 1.

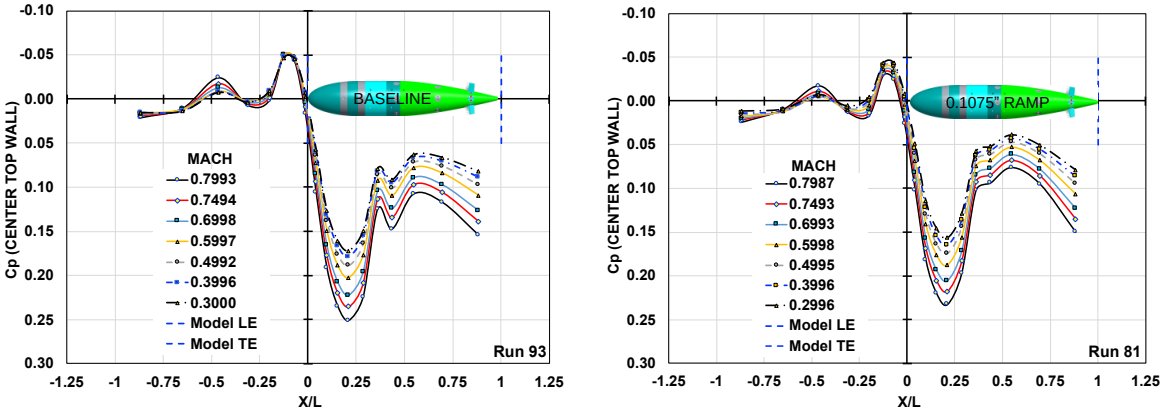

a) Baseline configuration b) 0.1075 Ramp configuration

Figure 12. Top test section wall pressure signature for two model configurations.

boundary layer was tripped at a prescribed distance from the model apex (or leading edge). The leading edge of the boundary layer manipulator is located at streamwise station of x/L=0.2677. Figure 13 shows the boundary layer growth for two configurations that were tested (baseline and 0.0825" tall ramp). The freestream Mach number and unit Reynolds number for these configurations were 0.75 and 26.3×10^6/ft, respectively. For many of the manipulator configurations, the measurements at the forward rake position suggest that the flow was still recovering from the boundary layer separation just behind the manipulator.

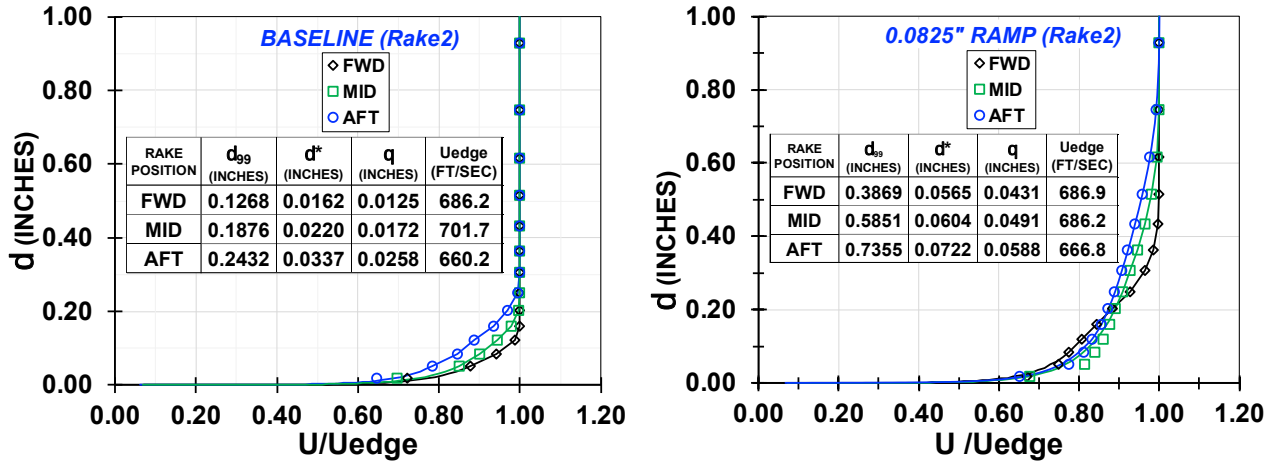

Figure 13. Comparison of the boundary layer development for manipulator ramp series 1 and 15.

Similar to the results shown in Figure 9, the boundary layer profiles do not exhibit an influence of Mach number. This is illustrated in Figure 14, which provides the boundary layer profiles obtained for Mach numbers ranging from 0.3 to 0.8.

A CFD comparison to the experimental baseline and 0.050" ramp configurations is shown in Figure 15. The agreement of the CFD and experimental data indicate that this is a good database for CFD comparisons. For the present work, a series of viscous grids were created that included

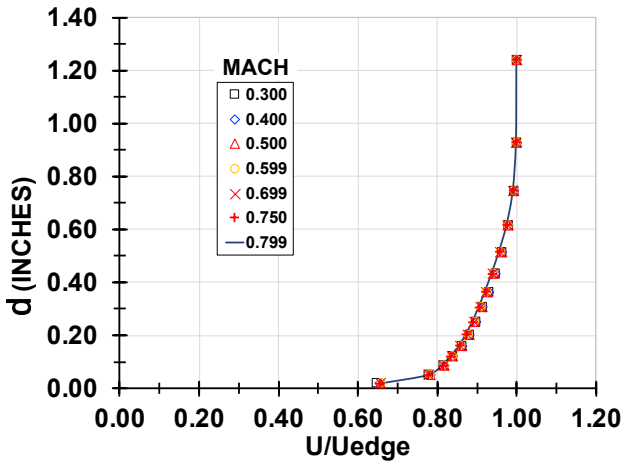

Figure 14. Velocity profiles for different Mach numbers for manipulator ramp series 15.

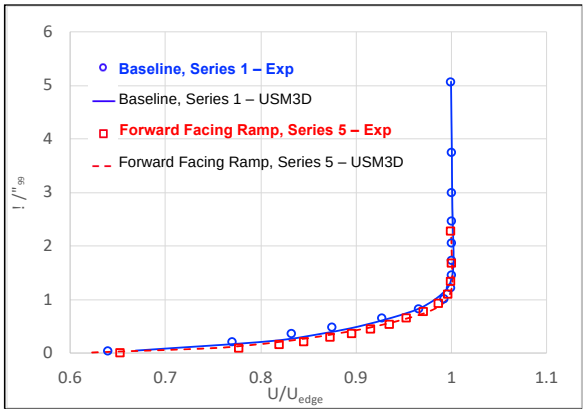

Figure 15. Comparison of boundary layer curve fits for manipulator ramp series 5 and rake 2, x/L=0.825.

the tunnel walls in their deformed state along with the semispan model mounted to the sidewall of test section. The flow solver used for the computational analyses is the USM3D flow solver[17]. USM3D is an unstructured, cell-centered Reynolds-averaged Navier-Stokes (RANS) flow solver developed at NASA Langley Research Center. Eleven CFD comparisons to this experiment are described in Reference 3.

For boundary layer flows with a uniform free stream, it has also been shown that experimentally measured turbulent boundary layers have velocity profiles very close to the mathematical expression of a power law having a fractional exponent (equation 8):

$$\frac{U}{U_\infty} \approx \left(\frac{z}{\delta}\right)^{1/n}. \tag{8}$$

For compressible flows, *n* varies from 4 to 12 depending on other flow parameters such as Mach number, Prandtl number, and wall to freestream temperature ratio. For the Mach range of this study, *n* is expected to be between 7 and 9.

In addition to evaluating the boundary layer profiles with a power law, a second method based on a law of the wall analysis was performed. Figure 16 shows a comparison of the Spalding's law of the wall to the power law described above. Comparing to the measured boundary layer profile, the law of wall data fit was superior to the power law fit. Both of these techniques indicate that the measured boundary layer is a fully developed turbulent boundary layer. Expanding the experimental data into wall functions, shown in Figure 17, indicates that the rake captured several data points in the inner layer.

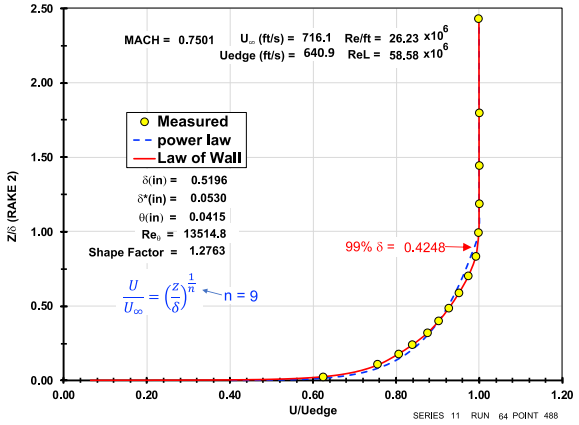

Figure 16. Comparison of boundary layer curve fits for manipulator pin series 11 and rake 2, x/L:0.825.

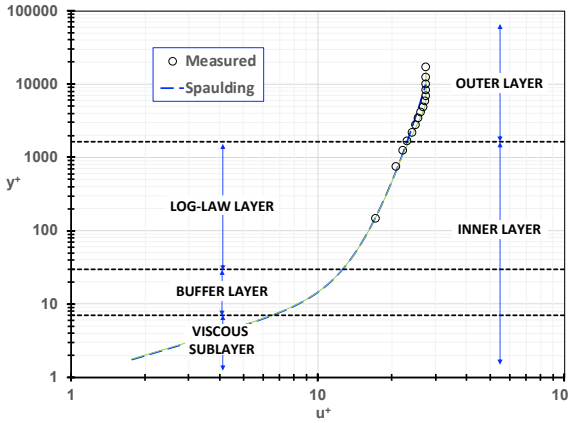

Figure 17. Example of wall functions using Spalding Law of Wall curve fit for manipulator pin series 11, x/L: 0.825.

To determine if the boundary layer is fully mixed and whether any undesirable flow instabilities were created due to the presence of the different manipulators, an assessment of the boundary layer was performed using an unsteady total pressure transducer having a bandwidth of 51.2kHz. The unsteady total pressure probe was located at three heights within of the boundary layer at an axial location corresponding to *x/L* = 0.825. The probe height was manually set to take measurements

at three different heights from the surface, corresponding to the edge of the boundary layer, middle of the boundary layer, and on the surface of the model.

Figure 18 compares the total pressure power density spectra for the three probe heights described above for Mach number and unit Reynolds number values of 0.75 and 26x10^6/ft. The spectra have been made dimensionless by using a reduced frequency based on unit length L and the edge velocity for the frequency and normalization of the magnitude by dynamic pressure. The broadband nature of this spectra indicates that the boundary layer is well mixed and does not have any residual coherent features that can be attributed to the manipulator. This spectra represents the same broadband character of all of the manipulators that were tested.

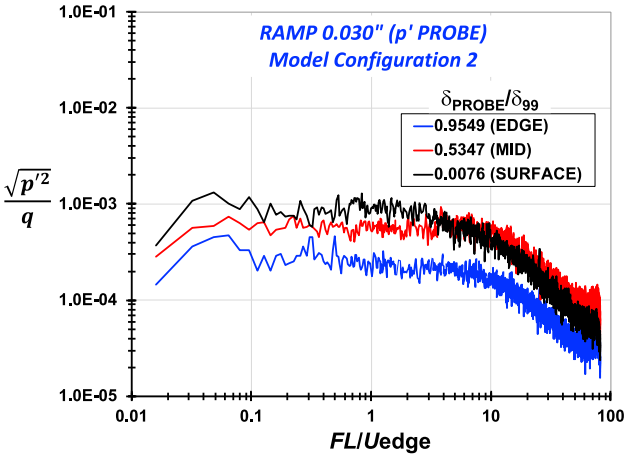

Figure 18. Boundary layer spectra for manipulator series 7, Mach=0.75, *U*edge = 624 ft/sec.

One of the goals of the experiment was to identify a manipulator configuration that would accomplish a target boundary layer height of 1.08 inches for an equivalent full-length fuselage of a single-aisle aircraft for the 0.3m TCT model scale. From the results shown in Figure 19, the ramp type manipulator requires a height of 0.14 inches to achieve the target boundary layer thickness. Similarly, the pin configuration results are summarized in Figure 20, which shows that the pin configurations considered were not able to accomplish the target boundary layer thickness. A summary of all 15 manipulator configurations considered for this test is provided in Table 2. The measurements on the bottom model configuration were limited because the boundary layer growth exceeded the rake height in the presence of the increased adverse pressure gradient highlighted in

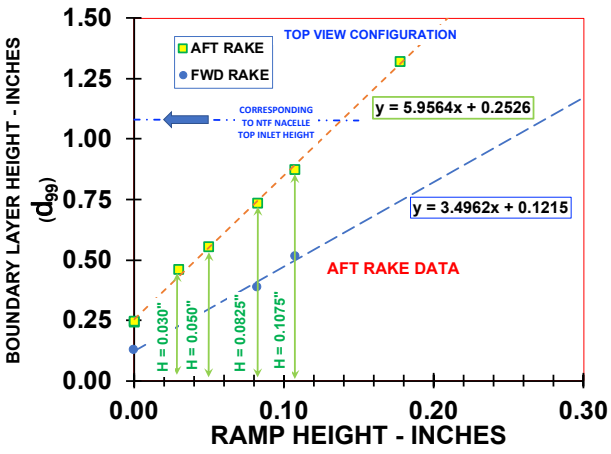

Figure 19. Projection of ramp heights to achieve target boundary layer profile.

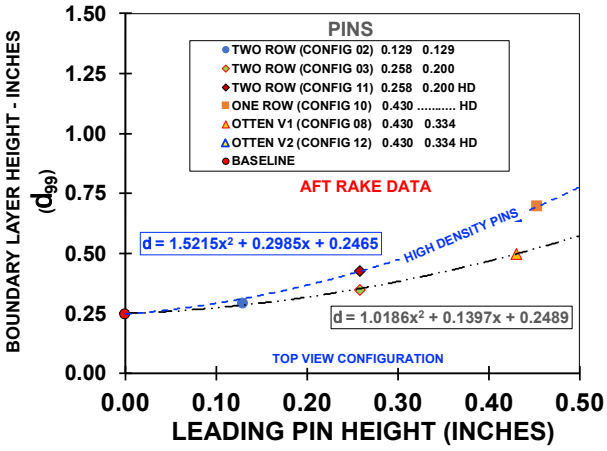

Figure 20. Projection of pin heights to achieve target boundary layer profile.

Figure 2. The baseline and smallest ramp manipulator were the only two manipulators that are considered valid for the bottom view model configuration.

Table 2. Boundary layer characteristics of different manipulators.

Config (VIEW)	Rake 2 Location	Series (Collar)	LaRC 0.3mTCT Front pin height (in)	LaRC 0.3mTCT Aft pin height (in)	Collar Description	d (in) 99% at Mach: 0.75	d* (in) at Mach: 0.75	q (in) at Mach: 0.75	Shape Factor	Re/ft $x10^6$
TOP	AFT	1	0.0000	0.0000	No Pins (BASELINE Rake2)	0.2465	0.0348	0.0267	1.3035	26.17
TOP	AFT	4	0.1500	NA	Single Short Row	0.3570	0.0478	0.0369	1.2948	26.39
TOP	AFT	10	0.4530	NA	Single Tall Row	0.6950	0.1041	0.0780	1.3346	26.32
TOP	AFT	2	0.1290	0.1290	Two Rows Same Height Short	0.2906	0.0307	0.0245	1.2517	26.23
TOP	AFT	3	0.2580	0.2002	Two Rows Var Height Med	0.3468	0.0443	0.0344	1.2878	26.25
TOP	AFT	11	0.2580	0.2002	Two Rows Var Height HD	0.4248	0.0530	0.0415	1.2763	26.23
TOP	AFT	8	0.4300	0.3336	Otton Height	0.4988	0.0629	0.0484	1.2980	26.27
TOP	AFT	12	0.4300	0.3336	Otton Height - High Density	0.6562	0.0889	0.0689	1.2172	26.21
TOP	AFT	9	0.0300	Aft Facing	AFT Ramp (0.0300")	0.4623	0.0491	0.0395	1.2422	26.26
TOP	AFT	6	0.0500	Aft Facing	AFT Ramp (0.0500")	0.5769	0.0591	0.0480	1.2314	26.39
TOP	AFT	7	0.0300	Fwd Facing	FWD Ramp (0.0300")	0.4361	0.0493	0.0393	1.2546	26.28
TOP	AFT	5	0.0500	Fwd Facing	FWD Ramp (0.0500")	0.5536	0.0571	0.0463	1.2319	26.28
TOP	AFT	15	0.0825	Fwd Facing	FWD Ramp (0.0825")	0.7355	0.0722	0.0588	1.2203	26.19
TOP	AFT	13	0.1075	Fwd Facing	FWD Ramp (0.1075")	0.8725	0.0864	0.0714	1.2107	26.21
TOP	AFT	14	0.1775	Fwd Facing	FWD Ramp (0.1775")	1.3200*	0.1202	0.0994	1.2090	20.14
TOP	AFT	1	0.0000	0.0000	No Pins (BASELINE Rake2)	0.2432	0.0335	0.0256	1.3053	26.20
TOP	FWD	1	0.0000	0.0000	No Pins (BASELINE Rake2)	0.1268	0.0157	0.0122	1.2930	26.07
TOP	FWD	15	0.0825	Fwd Facing	FWD Ramp (0.0825")	0.3869	0.0563	0.0430	1.3089	26.27
TOP	FWD	13	0.1075	Fwd Facing	FWD Ramp (0.1075")	0.5150	0.0745	0.0545	1.3671	26.06
TOP	FWD	12	0.4300	0.3336	Otton Height - High Density	0.4330	0.0625	0.0498	1.2554	26.22
TOP	MID	12	0.4300	0.3336	Otton Height - High Density	0.5493	0.0691	0.0547	1.2631	26.08
TOP	MID	15	0.0825	Fwd Facing	FWD Ramp (0.0825")	0.5851	0.0608	0.0495	1.2278	26.08
TOP	MID	13	0.1075	Fwd Facing	FWD Ramp (0.1075")	0.6923	0.0736	0.0598	1.2297	26.07
TOP	MID	1	0.0000	0.0000	No Pins (BASELINE Rake2)	0.1876	0.0220	0.0172	1.2741	26.18
BOTTOM	AFT	1	0.0000	0.0000	No Pins (BASELINE Rake2)	0.5655	0.1034	0.0721	1.4341	26.08
BOTTOM	AFT	7	0.0300	Fwd Facing	FWD Ramp (0.0300")	1.0472	0.1323	0.1011	1.3080	26.08
BOTTOM	AFT	15	0.0825	Fwd Facing	FWD Ramp (0.0825")	1.3496*	0.1805	0.1370	1.3178	20.05
BOTTOM	AFT	12	0.4300	0.3336	Otton Height - High Density	1.5000*	0.2688	0.1745	1.5404	26.08

*Denotes boundary layer exceeded rake height

Concluding Comments

The thickening of a turbulent boundary layer can be accomplished at transonic conditions using techniques that are presented in this paper. This paper highlighted the streamwise development and growth of the artificially thickened boundary layer for different manipulators that included both ramp type and pin type. Ramp type manipulators were shown to achieve a growth factor of up to 5.9 in the presence of a mild pressure gradient while maintaining boundary layer characteristics similar to a naturally developed turbulent boundary layer. The pin type manipulators were also effective in growing the boundary layer and had similar characteristics at 500 pin diameters but only achieved a growth factor of 2.78.

It is possible to integrate of these boundary layer manipulator techniques into technologies that are dependent on the growth of the boundary layer, such as Boundary Layer Ingestion. It is recommended to utilize ramp type manipulators instead of pin type manipulators since they are easier to fabricate and easier to predict. It is also recommended to utilize CFD techniques to include specific pressure gradients that are not represented in this paper.

Acknowledgements

The effort has been supported by the Advanced Air Transport Technology project (AATT) and Novel Propulsion Airframe Integration (NPAI) team. Special thanks are given to Scott Anders, Chris Hughes, and Anthony Nerone for their support and latitude in the design and testing of the 0.3m Transonic Cryogenic Tunnel boundary layer model. The successful testing of this model could not have been accomplished without the dedication, technical expertise, and energy of the 0.3m TCT technicians Mike Chambers, Tammy Jo Price, Karl Maddox, Reginald Brown, facility test engineer Cliff Obara, facility safety head Wesley Goodman, facility researcher S. Balakrishna, and facility manager Don Saxer.

.

References

[1] Welstead, J.R., Felder, J.L., "Conceptual Design of a Single-Aisle Turboelectric Commercial Transport with Fuselage Boundary Layer Ingestion," AIAA 2016-1027, January 2016.
[2] Gray, J., Mader, C.A., Kenway, K.W., Martins. J. R., "Approach to Modeling Boundary Layer Ingestion using a Fully Coupled Propulsion-RANS Model," AIAA Paper 2017-1753, January 2017.
[3] Mineck, R.E., "Hardware and Operating Features of the Adaptive Wall Test Section for the Langley 0.3-Meter Transonic Cryogenic Tunnel," NASA TM 4114, June 1986
[4] Bozeman, M., "USM3D Analyses in Support of the 0.3 Meter Wind-Tunnel Test of Boundary-Layer Thickener Configurations" AIAA paper, January 2020.
[5] Von Karman, T., "Mechanial Similitude and Turbulence," NACA-TM 611, March 1931.
[6] Schlichting, Hermann (1979). *Boundary-Layer Theory*, 7th ed., McGraw Hill, New York, U.S.A.
[7] Spalding D.B. "A single formula for the law of wall," J. Appl. Mech., vol.28, Ser. E, pp.455-458, (1961).
[8] Keller, J.B., "Power Laws for Turbulent Boundary Layer Flow," Physics of Fluids, Vol.14, No. 12, November 2002.
[9] G.I. Barenblatt, ''Scaling laws for fully developed shear flows. Part I: Basic hypotheses and analysis,'' J. Fluid Mechanics, Vol. 248, No. 513, 1993.
[10] Otten, L.J., Van Kuren, J.T., "Artificial Thickening of High Subsonic Mach Number Boundary Layers," AIAA Journal, Vol.14, No. 11, November 1976.
[11] Johnson, D. F. and Mitchell, G. A., "Experimental Investigation of Two Methods for Generating an Artifically Thickened Boundary Layer," NASA, TM X-2238, April 1971.
[12] Kilgore, R.A., and Dress, D.A.: The Application of Cryogenics to Hight Reynolds Number Testing in Wind Tunnels. Part1: Evolution, Theory, and Advantages Cryogenics, Vol. 24, August 1984, pp. 395-402.
[13] Balakrishna, S., Kilgore, A.W., Performance of the 0.3-Meter Transonic Cryogenic Tunnel with Air, Nitrogen, and Sulfur Hexafloride Media Under Close Loop Automatic Control, NASA Contractor Report 195052, January 1995.
[14] Foster, Jean M., Adcock, Jerry B., "Users Guide for the National Transonic Facility Research Data System", TM-110242, April 1996.
[15] Beattie, James A.; and Bridgeman, Oscar C.: A New Equation of State for Fluids. The Journal of American Chemical Society Vol. 50, No. 12, December 1928.
[16] Klebanoff, P. S. and Diehl, Z. W., "Some Features of Artificially Thickened Fully Developed Turbulent Boundary Layers with Zero Pressure Gradient," NACA, Rept. 1110, 1954.
[17] Frink, N. T., "Tetrahedral Unstructured Navier-Stokes Method for Turbulent Flows," AIAA Journal, Vol. 36, No. 11, 1998, pp. 1975–1982.